ACS APPLIED MATERIALS & INTERFACES

Research Article

www.acsami.org

Photovoltachromic Device with a Micropatterned Bifunctional Counter Electrode

Alessandro Cannavale,[†] Michele Manca,*[,†] Luisa De Marco,[†] Roberto Grisorio,[∥] Sonia Carallo,[‡] Gian Paolo Suranna,[∥] and Giuseppe Gigli[†,‡,§]

[†]CBN, Center for Biomolecular Nanotechnologies, Fondazione Istituto Italiano di Tecnologia - Energy Platform Via Barsanti, 73010 Arnesano, Lecce, Italy

[‡]NNL, National Nanotechnology Laboratory, CNR Istituto Nanoscienze, c/o Distretto Tecnologico, Via Arnesano km 5, 73100 Lecce, Italy

[§]Dipartimento di Matematica e Fisica "E. De Giorgi" - Università del Salento, via per Arnesano, 73100 Lecce, Italy

[∥]DICATECh - Dipartimento di Ingegneria Civile, Ambientale, del Territorio, Edile e di Chimica - Politecnico di Bari- Via Orabona, 4 I-70125 Bari, Italy

ABSTRACT: A photovoltachromic window can potentially act as a smart glass skin which generates electric energy as a common dye-sensitized solar cell and, at the same time, control the incoming energy flux by reacting to even small modifications in the solar radiation intensity. We report here the successful implementation of a novel architecture of a photovoltachromic cell based on an engineered bifunctional counter electrode consisting of two physically separated platinum and tungsten oxide regions, which are arranged to form complementary comb-like patterns. Solar light is partially harvested by a dye-sensitized photoelectrode made on the front glass of the cell which fully overlaps a bifunctional counter electrode made on the back glass. When the cell is illuminated, the photovoltage drives electrons into the electrochromic stripes through the photoelectrochromic circuit and promotes the Li^+ diffusion towards the WO_3 film, which thus turns into its colored state: a photocoloration efficiency of 17 cm^2 min^{-1} W^{-1} at a wavelength of 650 nm under 1.0 sun was reported along with fast response (coloration time <2 s and bleaching time <5 s). A fairly efficient photovoltaic functionality was also retained due to the copresence of the independently switchable micropatterned platinum electrode.

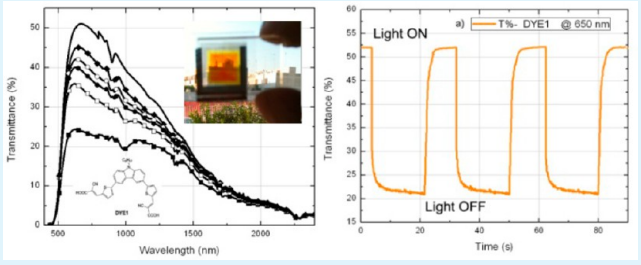

KEYWORDS: *solar control, smart window, photovoltachromic cell, micropatterned counter electrode, photocoloration efficiency, dye-sensitized electrode*

1. INTRODUCTION

The availability of affordable, efficient, and easily up-scalable photovoltaic (PV) technologies is a pivotal challenge in view of an upcoming diffusion of a next generation of building-integrated energy conversion systems.[1,2] In this respect, during the last two decades, dye-sensitized solar cells (DSSCs) have attracted widespread academic and industrial interest because, in comparison to silicon based technologies, they can be manufactured using low cost materials[3] and relatively easy fabrication processes, often borrowed from the printing industry. These issues alone, however, do not constitute a sufficient and effective driving force toward the full scale industrialization of DSSC technology. Competition with silicon-based PV technologies in terms of cost-effectiveness has become hardly sustainable. Energy production costs of silicon-based photovoltaic modules, in fact, dropped from 1.00$/W in 2009 to 0.35$/W in 2012.[4] So current state-of-the-art DSSCs do not represent an immediate economic advantage in the challenge for large-scale PV production.

On the other hand, DSSC could constitute a winning technology in the perspective of exploiting their unique characteristics in specific market niches, which means, for instance, through the design and the implementation of a new generation of smart photoelectrochemical devices capable of integrating two or even more different functionalities.

In the last two decades, considerable research efforts have been directed towards materials and devices intended for the dynamic solar control of buildings, often referred to as 'smart windows' or 'switchable glazings'[5] in general, 'smart' devices can react to external stimuli by modifying their behavior in response to the variation of some specific external conditions. Electrochromic cells (EC)[6] are smart devices that undergo reversible and persistent changes of their optical properties, when a voltage is applied to them. The interest in this field was boosted in the mid-1980s with the realization that electrochromism in

Received: October 29, 2013
Accepted: January 24, 2014
Published: January 24, 2014

   dx.doi.org/10.1021/am404800m | ACS Appl. Mater. Interfaces 2014, 6, 2415−2422

advanced architectural glazings[7,8] could be an effective technology to improve energy efficiency in buildings, prefiguring the real feasibility of the "smart" window, with variable transmittance of light and solar energy. Since then, electrochromism has remained an active area for basic and applied research, with large possibilities for uses in emerging technologies. Electrochromic materials and related devices can rightly be considered a subset of the "solar energy materials". It should be highlighted indeed that building integrated "smart" windows are able to improve two features that are often thought of as incompatible: energy efficiency (i.e. by reduction of air conditioning needs) and indoor comfort, due to the attenuation of glare probability and undesired solar gains.[9] An electrochromic device generally presents a sandwich architecture in which a conductor is embedded between a chromogenic electrode and a transparent conductor both of them realized onto a glass substrate. The electrochromic films transports both ions and electrons, thus belonging to the class of mixed conductors. On the other hand, the transparent conductors only transport electrons. Optical absorption occurs when electrons penetrate the electrochromic films and, simultaneously, cation intercalation takes place. Electrons are then captured by metal ions with modifications of their oxidation state; these "extra" electrons absorb photons from the incident light to give them enough energy to jump to neighboring metal ion sites.[10]

In 1996 Bechinger et al.[11] implemented an electrochromic layer within a dye-sensitized solar cell and for first realized what is today known as a photoelectrochromic cell (PEC), i.e. an electrochemical cell consisting of two electrodes −an electrochromic cathode and a mesoporous photoanode − coupled by an iodine/iodide based electrolyte. The dye-sensitized photoelectrodes power the coloration of the electrochromic counter electrode, in response to the photovoltage generated by the incoming solar radiation.[12] In this configuration, the photovoltage produced by the dye sensitized electrode drives electrons and compensates the charge of Li^+ ions migrating within the WO_3 film,[13−15] resulting in the coloration of the EC film. The coloration process is equivalent to charging a battery: the photovoltage generated by the dye-sensitized electrode is used to charge the EC layer. The coloration process is activated by the solar irradiance, without using any external energy source.

Some years later Georg et al.[16] proposed an alternative device architecture: the dye-covered nanoporous TiO_2 layer was deposited on the porous WO_3 layer and the counter electrode was in this case constituted by a Pt film. The pores of the TiO_2 and WO_3 layers were filled with a liquid electrolyte. After photon absorption by the dye, electrons are rapidly injected from the excited state of the dye into the conduction band of the TiO_2 and diffuse into the WO_3.[17] Following the injection of photogenerated electrons, Li^+ ions intercalate into the WO_3 leading to its coloration from transparent to blue. The device bleaches when short-circuited or as a consequence of an irradiance attenuation.

Numerous other device architectures have been explored during the last decade[18−22] and several polymeric materials have been used as electrochromic layers as well as poly(3,4-ethylenedioxythiophene) (PEDOT)[23] and polyaniline (PANI).[24]

On the basis of the aforementioned considerations, the natural technological evolution of this class of devices should be represented by an integrated photovoltaic powered electrochromic (PV−EC) window, also considering that the operational characteristics of both PV and EC technologies are highly compatible.[25] A small area of PV cells could in fact provide sufficient electric power to operate a large-area EC window. In the course of the last years just a couple of design options have been explored in this context. The first demonstration of a reliable approach to conveniently integrate PV and PEC technologies has been reported in 2009 by Wu et al.[26] A new device architecture was proposed, namely a photovoltachromic cell (PVCC) capable of modulating its optical transmittance with no need for an external energy supply, and of simultaneously producing electrical power by photovoltaic conversion, since it also operates as a DSSC. The energy conversion efficiencies reported for this first demonstration of PVCC was ∼0.5% and it was not possible to separately manage PV and PEC functionalities.

In a previous work, we have recently implemented a self-powered highly performing dye-sensitized PVCC implementing an engineered bifunctional counter electrode made by a C-shaped platinum frame which surrounds a square WO_3-coated region.[27] On the conductive side of the front-on glass, a C-shaped photoelectrode was correspondingly realized in such a way as to be overlapped to the platinum frame. So, two separated areas of the counter electrode (the catalytic area and the electrochromic film) share the same photoanode and are connected to it by means of two external circuits which can be independently switched, thus activating (either separately or jointly) the photovoltaic and the photoelectrochromic features of the device.

Even though this device integration led to a significant enhancement of the photovoltaic performances with respect to the state-of-the-art, as well as to a remarkable improvement of the coloration kinetics, some important aspects still needed investigation: firstly, the region covered by the platinum catalyst cannot undergo a chromic modulation; moreover, the uniformity and kinetics of the coloration process strongly depends on the distance from the platinum layer.

We deemed it worthwhile to address these issues recently focusing on the development of a new PVCC architecture based on the exploitation of a full area bifunctional counter electrode, in which the catalytic and electrochromic regions are arranged to form an interdigitated array of microsized stripes, which is totally overlapped to a partially transparent dye-sensitized photoelectrode fabricated on the front-side glass of the "sandwich" device, as schematically depicted in Figure 1. In this work, we describe the fabrication procedure of color-controllable PVCCs devices of this kind, sensitized with two suitably chosen dyes and discuss their full electro-optical characterization.

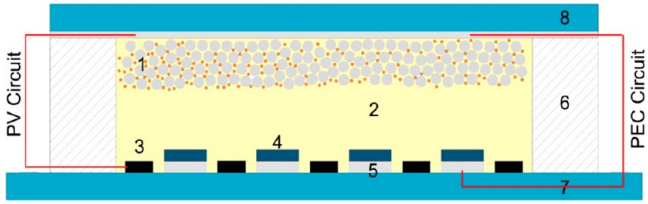

Figure 1. Cross-section of the device: 1. dye sensitized transparent TiO_2 photoelectrode; 2. electrolyte; 3. platinum stripes; 4. and 5. ITO/WO_3 pattern; 6. sealant; 7. float glass substrate; 8. conductive glass substrate.

2. EXPERIMENTAL SECTION

2.1. Fabrication of the Micropatterned Bifunctional Counter Electrode. A multistep fabrication process was designed and set-up to realize two distinct (and electrically separated) comblike electrodes onto a soda-lime glass substrate. A schematic view of the main fabrication steps is sketched in Figure 2.

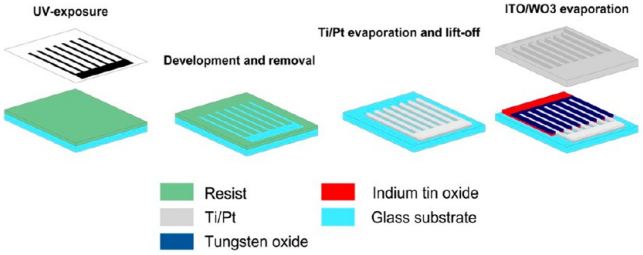

Figure 2. Fabrication of the interdigitated counter electrodes: a) photolithographic process consisting of UV-irradiation of the photoresist through a shadow mask; b) photoresist development and removal of the exposed pattern; c) electron-beam evaporation of a platinum layer and and removal of the photoresist. d) electron-beam evaporation of the ITO and WO_3 layers through a physical mask.

A photolithographic approach was adopted to obtain the suitable pattern for the Platinum stripes. A photoresist coating was performed on bare glass substrates, which were exposed to UV light using a specifically designed photomask. Once the UV-exposed photoresist (AZ5214E from CLARIANT) was removed, the catalyst stripes consisting in 3 nm of titanium (which served as adhesion promoter) and 20 nm of platinum were deposited as a thin film, by electron beam evaporation (Temescal Supersource), after evacuating the chamber to 10^{-7} mbar. The rate of platinum deposition was about 1.0 Å/s and the e-beam power was ~38%. The fabrication step of the platinum area of the counter electrode was completed by removing the unexposed photoresist mask by dipping the film in acetone for 5 minutes.

After completion of the Pt pad deposition process, a suitably designed steel laser-cut physical mask was used to realize the electrochromic region (namely the WO_3 and ITO layers) of the counter electrode. High vacuum e-beam deposition was selectively performed to obtain an interdigitated pattern of 150 nm thick ITO, which was used as a conductive underlayer for controlling the electrochromic functionality. In this case, the vacuum chamber was initially evacuated to 10^{-7} mbar and then a pure dry oxygen flux (5 sccm) was admitted through a needle valve. The pressure was maintained at 10^{-4} mbar throughout the deposition. The rate of deposition was ~0.5 Å/s and the substrate temperature was maintained at 245 °C. Before carrying out the subsequent WO_3 evaporation, the collecting stripe at the extremity of the ITO pattern was covered by using an aluminium mask in order to keep a rectangular pad to be used as electrical contact for the electrochromic region (see Figure 3).

The 300 nm thick WO_3 layer was deposited (chamber pressure: 10^{-4} mbar, deposition rate: 0.5 Å/s, substrate temperature: 215 °C, oxygen flux: 20 sccm) through the steel physical mask. Figure 3 shows electron micrographs and relevant geometrical features of the interdigitated pattern obtained after completion of the counter electrode fabrication.

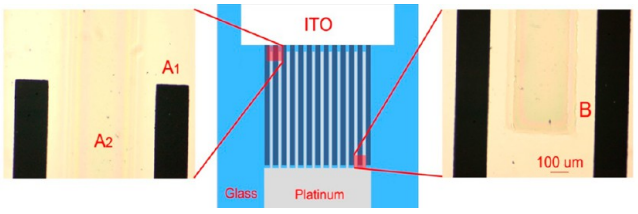

Figure 3. Geometry of the bifunctional counter electrode and electron micrograph images showing the spacing between ITO/WO_3 and Pt patterns. A_1 represents the width of Pt stripes; A_2 is the width of WO_3/ITO stripes; B is the gap between the Pt stripes and the WO_3/ITO.

The widths A_1 and A_2 of the Ti/Pt and ITO/WO_3 stripes are 250 μm and 500 μm, respectively; the distance between two neighboring stripes B (which is the portion of bare inactive glass) was of ~100 μm, which guarantees an effective electrical separation. The stripes length was 1.40 cm, whereas the overall width of the counter electrode was 1.85 cm.

2.2. Photovoltachromic Cells Fabrication. Fluorine-doped tin oxide (FTO) glass plates (15 Ω/sq, Xin Yan Technology LTD) were first cleaned in a detergent solution using an ultrasonic bath for 15 min and then rinsed with water and ethanol. For the fabrication of the TiO_2 photoelectrodes, nanorods-based pastes[28] were deposited by doctor-blade on a 1.0 cm^2 area to produce highly transparent 5 μm-thick films. The films were gradually heated under an air flow and sintered at 450 °C for 30 min. The substrate temperature was then allowed to slowly decrease, and, at ~80 °C, they were immersed into the dye solution.

To this purpose, two different dyes were chosen in order to conduct the present investigation: the well-known Ru(III) based sensitizer N719 and the DYE1, a donor−acceptor dibranched fully organic dye which has been recently proposed by us.[29] The following dye solutions were used for the sensitization process: 0.2 mM of N719 in acetonitrile/tert-butanol 1:1 and 0.2 mM of DYE1 in ethanol.

A suitable redox electrolyte was also formulated in order to optimize the performances of the counter electrode in the photovoltachromic devices. Preliminary investigations allowed to find the right compromise between the photovoltaic and the photoelectrochromic performances using the following electrolyte composition: 0.7 M LiI, 0.03 M I_2, and 0.3 M 4-*tert*-butylpyridine (4TBP) in acetonitrile.

The photovoltachromic cell was assembled by facing the patterned Pt/WO_3 counter electrode to the semitransparent dye-sensitized photoelectrode using a suitably cut 50 μm thick Surlyn hot-melt gasket for sealing. The redox electrolyte was vacuum injected into the space between the electrodes through holes pre-drilled on the back of the counter electrode. The holes were eventually sealed using Surlyn hot melt film and a cover glass.

2.3. Electro-Optical Characterization. Optical transmittance spectra of the devices were measured by a VARIAN 5000 spectrophotometer in a wavelength range between 300 and 2500 nm. Full spectrum measurements and cyclic measurements of coloration/bleaching times were obtained applying biases (corresponding to different irradiance levels) to the device, using a Keithley 2420 source meter.

Coloration response times were obtained by monitoring the transmittance at a wavelength of 650 nm. This figure of merit was assessed by irradiating the short-circuited device using an array of seven white Luxeon LED (Cool White- 6500K, 7 LED 40 mm -1540 lm @ 700 mA) switched on at t = 1 s operated by the above mentioned source meter.

The ITO and the Pt pads showed a sheet resistance of 13.0 Ω/□ and 5.9 Ω/□, respectively, as assessed by four-point probe measurements, carried out adopting the Van der Pauw method in probe station.

In order to assess the photovoltaic performances, current−voltage (J−V) characteristics of the PVCCs were measured under AM 1.5 illumination at 100 mW cm^2 in Standard Test Conditions.

3. RESULTS AND DISCUSSION

Keeping a good transparency in the visible range represents an indispensable feature for a photovoltachromic window. Therefore, the first screening in the designing of the fundamental components of the PVCC was aimed at finding the suitable balance between the transparency in the bleached state and the solar energy conversion efficiency. To this purpose, the catalyst coverage factor was systematically tuned by changing the width of the platinized stripes as well as their separation, prior to

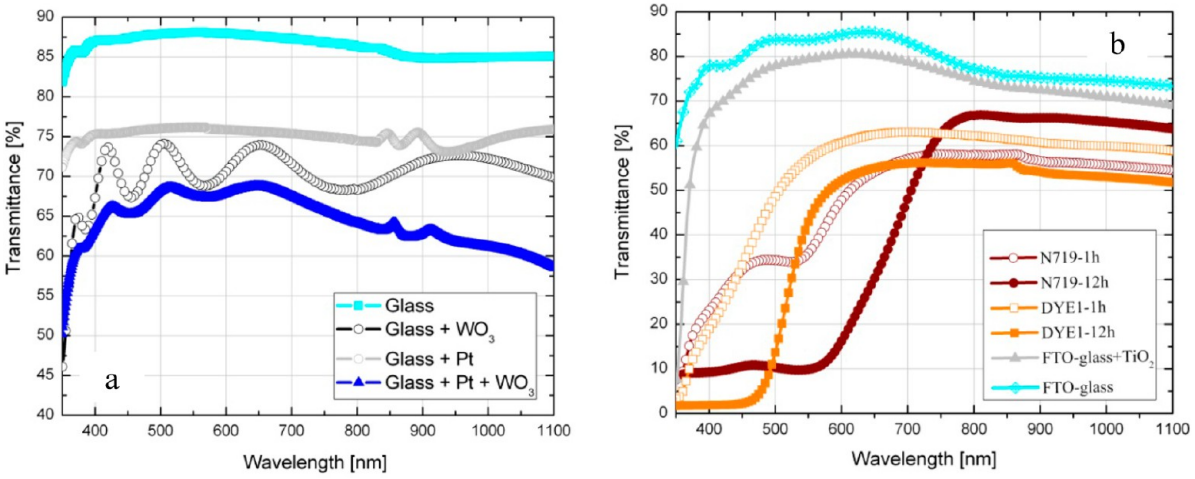

Figure 4. Transmittance spectra of the counter electrode a) and of the photoelectrode b) at different steps of the fabrication process.

proceeding with the interposition of the electrochromic electrode.

The width of the Pt microstripes was thus defined in such a way as to provide an area of the catalyst region sufficiently large to warrant an adequately efficient reduction of the I_3^- species. The optimal coverage factor was found to be ~1/3 with respect to the active area of the photoelectrode.

Transmittance spectra of the counter electrode were recorded after each step of the fabrication process and reported in Figure 4a. Main transparency losses are due to light reflection from the platinized strips. The addition of the electrochromic comb-pattern (ITO+WO_3) leads to a further transmittance reduction which is associated both to interference effects at the interface and to the non negligible absorption coefficient of the coating, especially in the red/near-infrared region. However, the overall transparency of the counter electrode has been kept at an acceptable level, which is ~65% in the visible range.

On the other side, an adequate consideration of the absorption prerogatives of the photoelectrode was necessary. A 5 μm thick mesoporous TiO_2–nanorods based film was deposited onto the FTO coated glasses and loaded with two different sensitizers, namely the well-known ruthenium-complex N719 and the fully organic dye DYE1,[29] constituted by a branched D(-π-A)$_2$ structure containing a rigid alkyl-functionalized carbazole core as the donor part, a thiophene units as the π-bridge, and a cyano-acrylic moiety as acceptor and anchoring part. The DYE1 showed peculiar features that made it very interesting in the framework of the present investigation: its absorption spectrum is in fact limited to the blue-green region (with a cut-off wavelength at ~500 nm) and hence, while retaining a good efficiency as sensitizer, allows a sensitively wider transmittance window with respect to N719 as deduced by inspection of Figure 4b, reporting the transmittance recorded at different steps of the counter electrode fabrication process.

After a 1 h dye-loading process the N719-sensitized film exhibited a transparency superior to 25% in the blue-green region and superior to 50% in the red/near-IR region, whereas after a fully sensitization process (which approximately takes 12 h) an almost complete saturation of the absorption in the full visible range nm was detected. We thus decided to employ a partially sensitized electrode for the construction of the N719-based PVCCs.

Conversely, after 1 h of up-taking process the DYE1-sensitized film exhibited an insufficient light harvesting capability resulting in a weak reduction of the transparency with respect to the bare unsensitized TiO_2 film. It instead effectively absorbed the incoming solar radiation in the range 400−500 nm after a complete dyeing process. We thus opted to use a fully sensitized electrode in the case of DYE1.

Then, the electrocatalytic properties of the comb-like platinum pattern were also evaluated through a comparison with a conventional full-area (~1 cm^2) platinum film deposited onto a commercial ITO-coated glass, which was used as reference. Table 1 shows the photovoltaic performances of four

Table 1. PV Performances of Four Different Semitransparent DSSCs

CE	dye	FF	Voc [V]	Jsc [mA cm^{-2}]	PCE[%] @1sun
full area	N719	0.64	0.74	6.28	2.97
comb-like	N719	0.46	0.70	5.97	1.92
full area	DYE1	0.63	0.72	6.40	2.90
comb-like	DYE1	0.45	0.68	6.02	1.84

DSSCs fabricated with the above mentioned 5 μm-thick semitransparent photoelectrode. DSSC embodying the comb-like counter electrodes exhibited, as expected, slightly lower photocurrent densities and led to extremely low fill factor values (0.45 and 0.46 for N719 and DYE1, respectively) with respect to those fabricated with the full-area Pt counter electrode.

Thereafter, if one considers the performances of the semitransparent TiO_2-nanorods-based photoelectrodes, it can be observed that the fully-sensitized DYE1 produces even a slightly higher photocurrent density with respect to the partially-sensitized ruthenium-based complex, despite the considerably wider absorption spectrum which characterizes the latter. The monochromatic incident photon-to-current conversion efficiency (IPCE) of DSSC embodying comblike counter electrodes was also measured and reported (Figure 5) as a function of the excitation wavelength. Inspection of the IPCE spectra provides a detailed explanation for the similar photocurrent densities observed for the two differently sensitized photoelectrodes. It can be noticed in fact that whereas DYE1 shows a sensitively better yield than N719 if stimulated at wavelengths below 520 nm (with an average IPCE

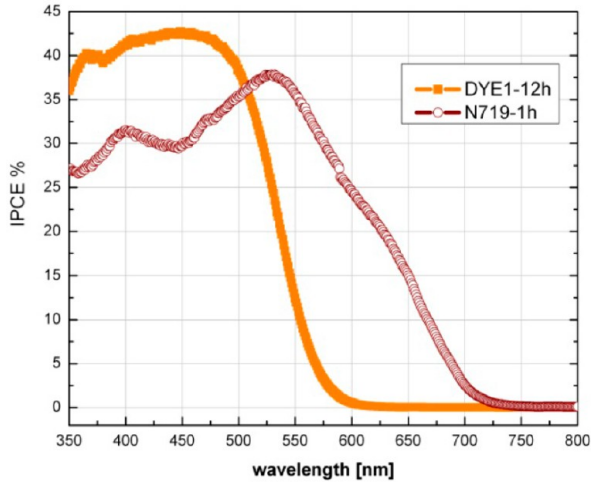

Figure 5. IPCE characteristics of the DYE1- and N719-sensitized DSSCs with comb-like counter electrodes.

of ~50%), the IPCE curve obtained for N719 subtends a higher area for wavelengths above this value.

We then systematically investigated the photovoltaic and photoelectrochromic behavior at different illumination intensities (1, 0.8, 0.6, 0.5, and 0.3 sun). The results are reported in Figure 6.

As expected, a drop in the short circuit current with the decrease of illumination intensity was detected in both cases as a consequence of the reduced number of absorbed photons. The value of V_{OC} also decreased at lower light intensities: it follows in fact a logarithmic dependence from the short circuit current J_{SC}, proportional to the light intensity.[30] It should be highlighted however that DYE1 exhibited a less remarkable drop of J_{SC} with respect to its ruthenium-based counterpart as a consequence of its higher molar extinction coefficient. This turned into an overcoming of the overall PCE at lower irradiance levels: below 0.8 sun in fact, DYE1-based PVCCs showed slightly better photovoltaic performances with respect to N719-based ones.

The photoelectrochromic circuit was eventually connected, and the modulation of the optical transmittance for DYE1 and N719-sensitized PVCCs was measured at the same levels of irradiance in the wavelength range between 450 and 2500 nm. The results are shown in Figure 7 (see Tables 2 and 3).

In this configuration, the photocurrent flow into the electrochromic region of the counter electrode leads to the Li ion intercalation in the WO_3 oxide stripes and to a chromic transition that depends on the generated photocurrent intensity, thus inducing a smart modulation of the optical transmittance (ΔT) which can finely be controlled by a modulation of the light intensity.

The DYE1-based cell revealed a higher ΔT throughout the visible spectrum mainly attributable to its higher transparency in the bleached state. An as high optical modulation as 32% at 650 nm under 1 sun was observed in comparison with a ΔT of 21% observed at the same wavelength for the ruthenium-based device.

Response times of the above referred PVCCs were also evaluated by subjecting the cells to alternate cycles of coloring and bleaching upon switching the electrical connection between the photoelectrode and the electrochromic stripes under 1 sun illumination.

As shown in Figure 8 the optical response of both N719- and DYE1-based devices is reported at 650 nm.

As soon as the PEC circuit is closed under illumination, an immediate drop of the transmittance is observed on a time scale of a few seconds. When the light is turned off, an as much fast bleaching process takes place, which occurs in less than 5 s. The observed fast bleaching time (one of the critical parameters for most state-of-the-art elecrochromic windows) is remarkable for a PVCC device. Such a fast responsivity is attributable to the comb-like geometry adopted for the counter electrode, in which nearby Pt stripes catalyze the I^- regeneration and, at the same time, promote the electron transfer from WO_3 to the electrolyte thus leading to the dramatic acceleration of the bleaching processes.

Another fundamental figure of merit in the characterization of chromogenic devices is represented by the Photocoloration Efficiency (phCE). We estimated this parameter by adopting the well-known relationship between the modulation of the optical density ΔOD and the solar energy density absorbed by the dye-sensitized photoelectrode to activate the complete transition from bleached to the colored state of the WO_3 stripes[18]

$$\mathrm{PhCE} = \frac{\Delta \mathrm{OD}}{G_T t} = \frac{\log\left(\frac{T_b}{T_c}\right)}{G_T t}$$

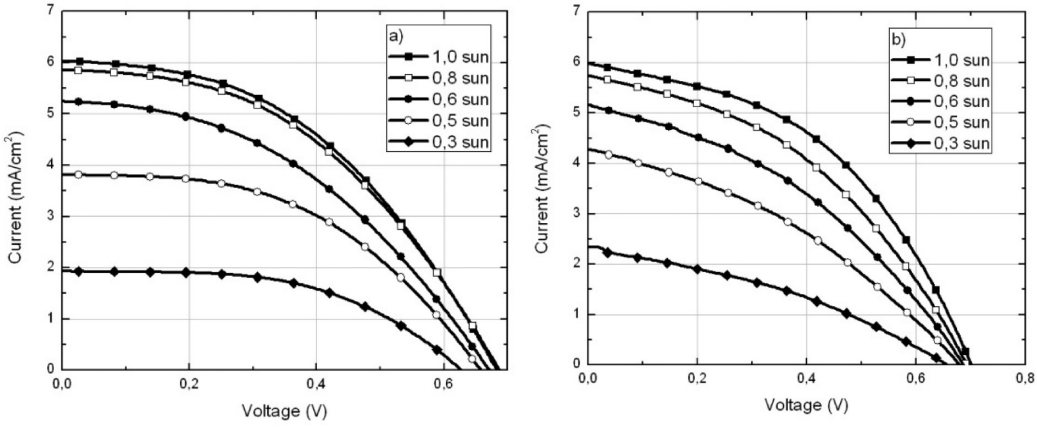

Figure 6. IV characteristics of the a) DYE1- and b) N719-sensitized PVCCs at different levels of irradiance.

dx.doi.org/10.1021/am404800m | ACS Appl. Mater. Interfaces 2014, 6, 2415−2422

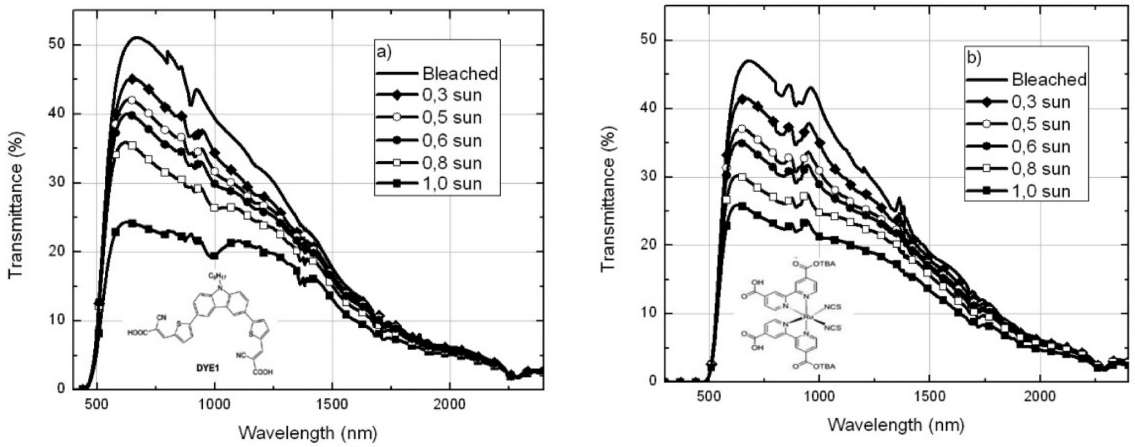

Figure 7. Transmittance spectra at different illumination levels for PVCC sensitized with DYE1 a) and N719 b).

Table 2. PV Performances of the DYE1-Sensitized PVCC at Different Levels of Irradiance

irradiance	FF	Voc [V]	Jsc [mA cm^{-2}]	PCE[%] @1sun
1.0 sun	0.45	0.68	6.02	1.84
0.8 sun	0.43	0.68	5.85	2.13
0.6 sun	0.42	0.66	5.24	2.42
0.5 sun	0.48	0.65	3.81	2.38
0.3 sun	0.52	0.62	1.93	2.06

Table 3. PV Performances of the N719-Sensitized PVCC at Different Levels of Irradiance

irradiance	FF	Voc [V]	Jsc [mA cm^{-2}]	PCE[%] @1sun
1.0 sun	0.46	0.70	5.97	1.92
0.8 sun	0.42	0.69	5.74	2.07
0.6 sun	0.39	0.68	5.14	2.26
0.5 sun	0.37	0.67	4.29	2.12
0.3 sun	0.36	0.65	2.33	1.80

where T_b and T_c correspond to the optical transmittance in the bleached and colored state, respectively, G_T is the total solar intensity for incidence normal to the device (expressed in W/cm^2), and t is the exposure time (expressed in minutes).

Figure 9 shows the photocoloration efficiencies of two above referred PVCCs. The DYE1-sensitized device shows higher photocoloration efficiencies throughout the visible spectrum and a lower cut-off wavelength as a consequence of the combined effect of its higher transparency in the bleached state and of its slightly superior photocurrent intensities at high illumination levels. The maximum value of phCE, corresponding to 17 cm^2 min^{-1} W^{-1} was recorded at wavelengths higher than 650 nm.

Images of the devices fabricated using DYE1 are reported in Figure 10, respectively in the bleached and colored condition.

CONCLUSIONS

We reported a novel photovoltachromic cell architecture based on an engineered bifunctional counter electrode consisting of two physically separated platinum and tungsten oxide regions, which are arranged to form complementary comblike patterns.

This counter electrode has been profitably combined with a specifically designed TiO_2-nanorods-based electrode sensitized with either N719 or an efficient blue-absorbing organic dye (DYE1). This device architecture, showing the best figures of merit when embodying the organic dye, represents the first demonstration of a fully integrated photovoltachromic device. Such an engineered architecture allows a twofold outcome: a self-powered fast-responsive control of the optical transmittance and electrical power generation through solar energy conversion. This new architecture provides a first step towards

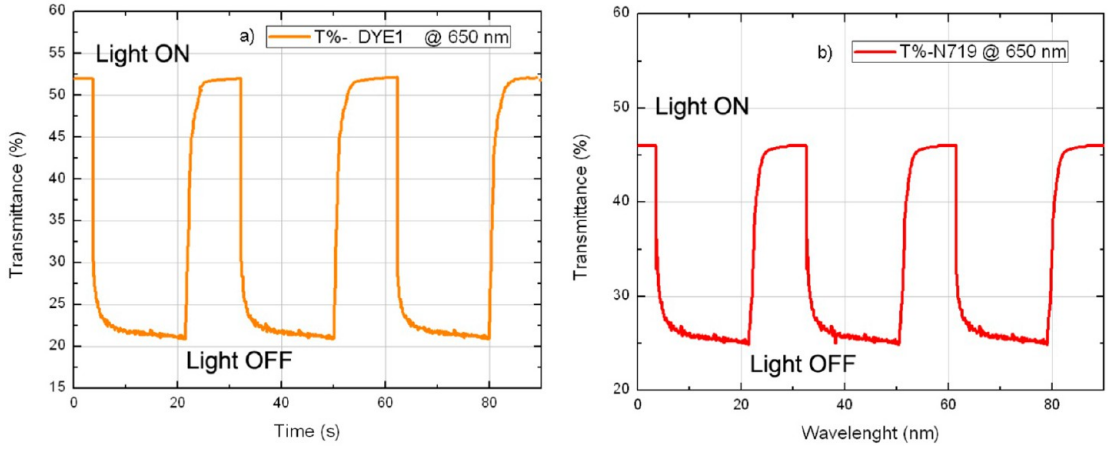

Figure 8. Coloring/bleaching cycles recorded under 1 sun illumination for PVCC sensitized with DYE1 a) and N719 b).

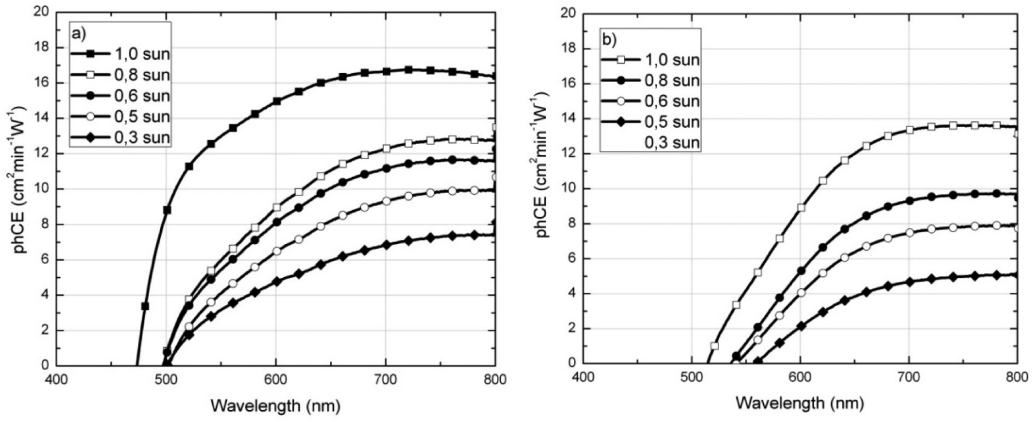

Figure 9. Photocoloration efficiency at different illumination levels of PVCCs sensitized with DYE1 (a) and N719 (b), respectively.

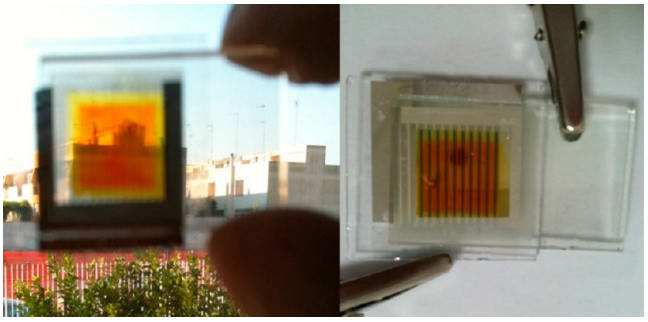

Figure 10. Pictures of a PVCC mounting a micropatterned bifunctional CE in the bleached (left) and in the colored state (right).

the development of large-area multifunctional smart windows to be integrated in the next generation of building glass facades.

AUTHOR INFORMATION

Corresponding Author

*E-mail: michele.manca@iit.it.

Author Contributions

The manuscript was written through contributions of all authors.

Notes

The authors declare no competing financial interest.

ACKNOWLEDGMENTS

This work has been partially supported by Regione PUGLIA (APQ Reti di Laboratorio, project "PHOEBUS" cod. 31) and by Italian Minister for Education and Research which funded the R&D program "MAAT" (PON02_00563_3316357 – CUP B31C12001230005). Cesare Bonserio from CentroLaser in Valenzano (Bari) and Diego Mangiullo from CNR-NANO in Lecce are kindly acknowledged for their precious technical support. Daunia Wind is also gratefully acknowledged for funding some correlated research activities on dye solar cells.

REFERENCES

(1) Hinsch, W.; Veurman, H.; Brandt, R.; Aguirre, L.; Bialecka, K.; Jensen, K. F. *Prog. Photovoltaics* **2012**, *20*, 698–710.

(2) Knaack, U. In *Research in Architectural Engineering Series - The Future Envelope 1: A Multidisciplinary Approach*; Knaack, U., Klein, T., Eds.; IOS Press: Netherlands, 2008; Vol. *8*, p 53.

(3) O'Regan, B.; Graetzel, M. *Nature* **1991**, *353*, 737–740.

(4) Bazilian, M.; Onyeji, I.; Liebreich, M.; MacGill, I.; Chase, J.; Shah, J.; Gielen, D.; Arent, D.; Landfear, D.; Zhengrong, S. *J. Renewable Sustainable Energy* **2013**, *53*, 329–338.

(5) Deb, S. K. *Sol. Energy Mater. Sol. Cells* **2008**, *92*, 245–258.

(6) Granqvist, C. G. *Sol. Energy Mater. Sol. Cells* **2012**, *99*, 1–13.

(7) Jaksic, N. I.; Salahifar, C. *Sol. Energy Mater. Sol. Cells* **2003**, *79*, 409–423.

(8) Granqvist, C. G.; Lansaker, P. C.; Mlyuka, N. R.; Niklasson, G. A.; Avendano, E. *Sol. Energy Mater. Sol. Cells* **2009**, *93*, 2032–2039.

(9) Tenner, A. D.; Zonneveldt, L. *Proceedings of "The Right Light 5" Conference*, 2002, Nice, France, session 11, pp 279–283

(10) Niklasson, G. A.; Granqvist, C. G. *J. Mater. Chem.* **2007**, *17*, 127–156.

(11) Bechinger, C.; Ferrere, S.; Zaban, A.; Sprague, J.; Gregg, B. *Nature* **1996**, *383*, 608–610.

(12) Gregg, B. A. *Endeavour* **1997**, *21* (2), 52–55.

(13) Zheng, H.; Ou, J. Z.; Strano, M. S.; Kaner, R. B.; Mitchell, A.; Kalantar-zadeh, K. *Adv. Funct. Mater.* **2011**, *21*, 2175–2196.

(14) He, T.; Yao, J. *J. Mater. Chem.* **2007**, *17*, 4547–4557.

(15) Balaji, S.; Djaoued, Y.; Albert, A. S.; Bruning, R.; Beaudoin, N.; Robichaud, J. *J. Mater. Chem.* **2011**, *21*, 3940–3948.

(16) Georg, A.; Opara Krasovec, U. *Thin Solid Films* **2006**, *502*, 246–251.

(17) Hauch, A.; Georg, A.; Baumgartner, S.; Opara Krasovec, U.; Orel, B. *Electrochim. Acta* **2001**, *46*, 2131–2136.

(18) Leftheriotis, G.; Syrrokostas, G.; Yianoulis, P. *Sol. Energy Mater. Sol. Cells* **2012**, *96*, 86–92.

(19) Yang, S.; Zheng, J.; Li, M.; Xu, C. *Sol. Energy Mater. Sol. Cells* **2012**, *97*, 186–190.

(20) Hechavarria, L.; Mendoza, N.; Rincon, M. E.; Campos, J.; Hu, H. *Sol. Energy Mater. Sol. Cells* **2012**, *100*, 27–32.

(21) Wua, C.; Hsu, C. Y.; Huang, K.; Nien, P.; Lin, J.; Ho, K. *Sol. Energy Mater. Sol. Cells* **2012**, *99*, 148–153.

(22) Hsu, C.; Lee, K.; Huang, J.; Justin Thomas, K. R.; Lin, J. T.; Ho, K. *J. Power Sources* **2008**, *185*, 1505–1508.

(23) Li, Y.; Hagen, J.; Haarer, D. *Synth. Met.* **1998**, *94*, 273–277.

(24) Huang, L. M.; Kung, C. P.; Hu, C. W.; Peng, C. Y.; Liu, H. C. *Sol. Energy Mater. Sol. Cells* **2012**, *107*, 390–395.

(25) Lampert, C. M. *Sol. Energy Mater. Sol. Cells* **2003**, *76*, 489–499.

(26) Wu, J.-J.; Hsieh, M.-D.; Liao, W.-P.; Wu, W.-T.; Chen, J.-S. *ACS Nano* **2009**, *3*, 2297–2303.

(27) Cannavale, A.; Manca, M.; Malara, F.; De Marco, L.; Cingolani, R.; Gigli, G. *Energy Environ. Sci.* **2011**, *4*, 2567.

(28) De Marco, L.; Manca, M.; Giannuzzi, R.; Malara, F.; Melcarne, G.; Ciccarella, G.; Zama, I.; Cingolani, R.; Gigli, G. *J. Phys. Chem. C* **2010**, *114*, 4228–4236.

(29) Grisorio, R.; De Marco, L.; Allegretta, G.; Giannuzzi, R.; Suranna, G. P.; Manca, M.; Mastrorilli, P.; Gigli, G. *Dyes Pigm.* **2013**, *98*, 221–231.

(30) Hara, K.; Horiguchi, T.; Kinoshita, T.; Sayama, K.; Sugihara, H.; Arakawa, H. *Sol. Energy Mater. Sol. Cells* **2000**, *64*, 115−134.